

Article

Deformation Analysis of Large Diameter Monopiles of Offshore Wind Turbines under Scour

Zhaoyao Wang¹, Ruigeng Hu¹, Hao Leng¹, Hongjun Liu^{1,2,*}, Yifan Bai³ and Wenyan Lu³

¹ College of Environmental Science and Engineering, Ocean University of China, Qingdao 266100, China; wangzhaoyao@stu.ouc.edu.cn (Z.W.); 11181011028@stu.ouc.edu.cn (R.H.); lh4517@stu.ouc.edu.cn (H.L.)

² Shandong Provincial Key Laboratory of Marine Environment and Geological Engineering, Qingdao 266100, China

³ School of Civil Engineering, Shandong Jianzhu University, Jinan 250101, China; 2018015150@stu.sdjzu.edu.cn (Y.B.); 2018015132@stu.sdjzu.edu.cn (W.L.)

* Correspondence: hongjun@ouc.edu.cn; Tel.: +86-532-66782571

Received: 27 July 2020; Accepted: 7 September 2020; Published: 28 October 2020



Abstract: The displacement of monopile supporting offshore wind turbines needs to be strictly controlled, and the influence of local scour can not be ignored. Using p–y curves to simulate the pile–soil interaction and the finite difference method to calculate iteratively, a numerical frame for analysis of lateral loaded pile was discussed and then verified. On the basis of the field data from Dafeng Offshore Wind Farm in Jiangsu Province, the local scour characteristics of large diameter monopile were concluded, and a new method of considering scour effect applicable to large diameter monopile was put forward. The results show that, for scour of large diameter monopiles, there was no obvious scour pit, but local erosion and deposition. Under the test conditions, the displacement errors between the proposed and traditional method were 46.4%. By the proposed method, the p–y curves of monopile considering the scour effect were obtained through ABAQUS, and the deformation of large diameter monopile under scour was analyzed by the proposed frame. The results show that, with the increase of scour depth, the horizontal displacement of the pile head increases nonlinearly, the depth of rotation point moves downward, and both of the changes are related to the load level. Under the test conditions, the horizontal displacement of the pile head after scour could reach 1.4~3.6 times of that before scour. Finally, for different pile parameters, the pile head displacement was compared, and further, the susceptibility to scour was quantified by a proposed concept of scour sensitivity. The analysis indicates that increasing pile length is a more reasonable way than pile diameter and wall thickness to limit the scour effect on the displacement of large diameter pile.

Keywords: pile foundations; offshore wind turbines; scour; p–y curve; finite difference method; horizontal displacement

1. Introduction

In offshore wind power projects, the foundation design accounts for about 25% of the total cost [1], and the foundation serviceability is of importance for the normal operation of wind turbines. Large diameter monopile (Figure 1) is widely used in practical engineering, with its advantages of superior economy and reliability [2].

Under the environmental loading from waves and currents, the displacement of monopile can not exceed 0.5° of rotation at the mudline, or another similar value suggested by the turbine manufacturers, so it is necessary to study the deformation characteristics of large diameter monopile under horizontal loads. Owing to the harsh environmental conditions and high cost, the field test of large diameter monopile is difficult to carry out, hence the numerical analysis is more commonly used. Bouzid et al. [3]

pointed out that the finite element method is effective for the assessment of lateral loaded monopile and the conventional p–y curve method derived from field tests of a small diameter is not suitable for large diameter monopile. Achmus et al. [4] evaluated the effect of pile diameter on p–y curves. Zhang et al. [5] proposed a p–y curve construction method for large diameter monopile, and takes the roughness of the pile–soil interface into account. Lee et al. [6] studied the cyclic effects on the p–y curve by centrifugal model test. Under the coupled waves and currents, local scour occurs around the pile foundation, which affects the static and dynamic response of monopile [7–9]. Therefore, the scour effect must be considered in the deformation analysis. He et al. [10] and Carswell et al. [11] reduced the buried depth of pile foundation by removing a certain depth of soil layer (Figure 2). Dai et al. [12] considered the scour pit features and introduced a wedge-shaped failure mechanism to express the influence of local scour.

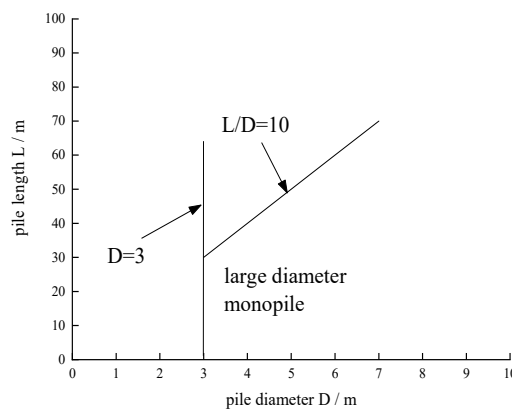


Figure 1. Generally accepted concept of large diameter monopile.

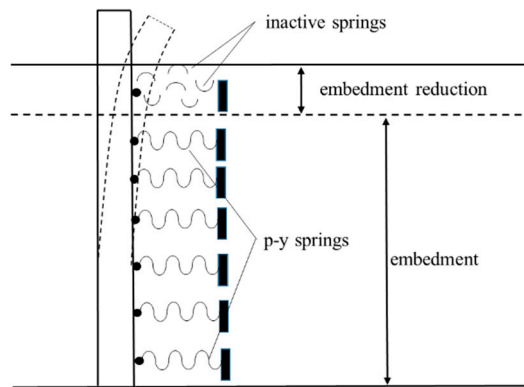


Figure 2. Embedment reduction diagram.

It can be seen that, for the analysis of large diameter monopile of offshore wind turbines, horizontal deformation characteristic is of significance, and appropriate methods should be selected. The p–y curve method is widely used and it is crucial to obtain the p–y curve suitable for large diameter monopile. Secondly, as for local scour, both the scour characteristic and scour effect consideration method lack the support of field data, as they only took the maximum scour depth into consideration instead of the scour pattern, and whether they are applicable to large diameter monopile remains uncertain. To quantitatively summarize the scour characteristics and the effect of large diameter monopile is helpful for offshore wind power construction and subsequent load and displacement analysis. In addition, few studies have focused on the displacement sensitivity of monopile under scour.

Therefore, this paper introduces the p–y curve method and the iterative procedure of finite difference method, and verifies the accuracy of the horizontal displacement analysis frame by model test and field test. Then, on the basis of the scour monitoring data from Dafeng offshore wind farm

in Jiangsu Province, we conclude the scour characteristics of large diameter monopile and propose a method of considering the scour effect applicable to large diameter monopile. Finally, by the proposed method, we extract p–y curves of monopile considering the scour effect through ABAQUS, and analyze the deformation characteristics of large diameter monopile under scour. The sensitivity of pile head displacement under scour is studied by analyzing the relationship among scour depth, pile head displacement, and pile parameters, and the concept of scouring sensitivity is proposed, which may provide ideas for practical engineering.

2. Deformation Analysis Method

2.1. p–y Curve

In the analysis of lateral loaded pile foundations, the soil is modeled as a system of uncoupled springs distributed along the depth, and the pile response can be obtained from the differential equation:

$$EI \frac{d^4y}{dx^4} + p(x) = 0 \tag{1}$$

where EI : pile bending stiffness, y : pile displacement, p : soil resistance, and X : length along the pile.

The key to solving the differential equation is the soil resistance function $p(x)$, which includes linear and nonlinear assumptions. The linear method assumes that the soil resistance p is proportional to the pile displacement y at any depth, which means the stiffness of soil spring could be represented by a constant. The other solution assumes that the soil resistance function $p(x)$ is non-linear, and the stiffness of soil spring could be described by p–y curves. Through field test or lab element test [13], the p–y curve at any depth under the mudline (Figure 3) could be constructed.

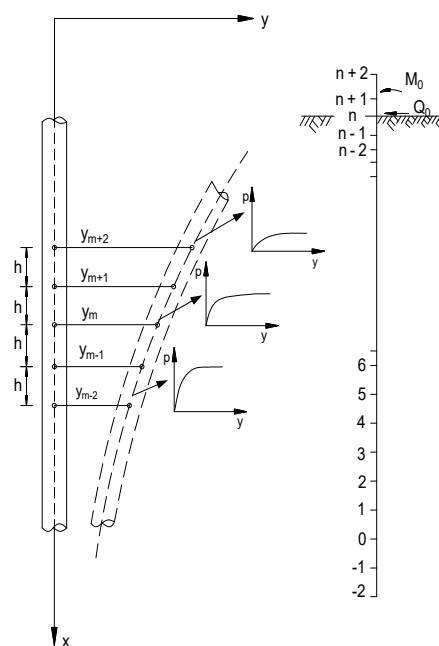


Figure 3. P–y curve at different depths and calculation diagram.

Matlock [14] and Reese et al. [15] proposed p–y curves for soft clay and stiff clay, respectively, and Reese et al. [16] gave the expression of p–y curves in sand. American Petroleum Institute’s recommendations [17] are widely used in practical engineering. Wang et al. [18] proposed a method applicable to both soft and stiff clay. Table 1 lists several p–y curve models, and Wang et al. [19] made a review on the p–y curve for monotonic and cyclic and discussed problems in existing studies.

Table 1. P–y curve empirical formula.

Soil Type	Expression	Notes
Soft clay (Matlock [14])	$\frac{p}{p_u} = 0.5\left(\frac{y}{y_{50}}\right)^{1/3}, y \leq 8$ $y_{50} \frac{p}{p_u} = 1, y > 8y_{50}$	p_u : ultimate soil resistance; y_{50} : displacement at half of the ultimate resistance
Clay (Wang et al. [18])	$\frac{p}{p_u} = \left(\frac{y/y_{50}}{a+by/y_{50}}\right), y \leq \beta$ $y_{50} \frac{p}{p_u} = 1, y > \beta y_{50}$	A, b, β : parameter obtained from triaxial test
Sand (API [17])	$p = Ap_u \tanh\left(\frac{K}{Ap_u} y\right)$	A : empirical factor; K : subgrade modulus, $K = kx$ (k is initial subgrade modulus; x is the distance to mudline)

2.2. Iterative Solution of Finite Difference Equations

Once the p–y curve is obtained, it is difficult to solve the differential equations by the analytical method. This paper solves the equations by finite difference iterative calculation [20]. The pile is divided into n segments (Figure 3), and the derivative deflection equation could be replaced by the difference equation:

$$y_{m-2} - 4y_{m-1} + \left(6 + \frac{E_s h^4}{EI}\right)y_m - 4y_{m+1} + y_{m+2} = 0 \tag{2}$$

After the process above, $n + 1$ difference equations would be obtained.

The shear force and moment of pile tip is 0, so the boundary conditions at pile tip is as follows:

$$y_{-2} - 2y_{-1} + 2y_1 - y_2 = 0 \tag{3}$$

$$y_1 - 2y_0 + y_{-1} = 0 \tag{4}$$

The shear force and moment of pile head are given as Q_0 and M_0 , so the boundary conditions at pile head are as follows:

$$y_{n-2} - 2y_{n-1} + 2y_{n+1} - y_{n+2} = \frac{2Q_0 h^3}{EI} \tag{5}$$

$$y_{n-1} - 2y_n + y_{n+1} = \frac{M_0 h^2}{EI} \tag{6}$$

With $n + 1$ equations along the pile length, 2 equations at the pile tip, 2 equations at the pile head, a total of $n + 5$ equations are obtained and then solved according to the matrix. Before solving the equations, a value of soil modulus E_{sm} should be pre-assumed and input to the iterative program, so that the pile displacement y could be output by solving the matrix, and thus the soil resistance p would be generated according to the corresponding p–y curves. Thus, the calculated soil modulus E_{sc} is obtained from the known p and y , and compared with E_{sm} . When the tolerance is small enough, the iteration stops and the calculation ends. Figure 4 shows the iteration flows and calculation algorithm.

2.3. Verification with Model Test

A model test was designed and then carried out to verify the accuracy of the method mentioned above. In the experiment, the deformation response of monopile in silt was obtained, and then it was compared with the result calculated by the p–y curve method.

2.3.1. Experiment Materials

The test chamber is a rectangle made of glass fiber reinforced plastics, and its size is annotated in Figure 5. The external walls are supported by three layers of steel angle to prevent deformation caused by excessive pressure in the chamber, and cardboard is padded between the steel angle and the test chamber.

The model pile is made of stainless steel pipe with an outer diameter of 32 mm, an inner diameter of 30.6 mm, and a length of 1.5 m. The bending stiffness of the model pile is 1510 N·m². Thirteen pairs of strain gauges of 120 Ω resistance were symmetrically set along both sides of the pile shaft and waterproofing was guaranteed. Eight pore pressure sensors were used to observe the dissipation of pore pressure in order to determine the degree of consolidation. The arrangement of strain gauges and pore pressure meters is shown in Figure 5.

The silt for the test is from the Yellow River Delta, and five groups of soil samples with depth of 10–50 cm under the mudline were taken and the average values of soil parameters are listed in Table 2. The undrained shear strength c_u measured by the vane shear test and the sieving curve are shown in Figure 6a,b.

Table 2. Soil parameters of model test.

Cohesion c (kPa)	Friction Angle φ (°)	Density ρ (g/cm ³)	Water Content ω (%)	Void Ratio e	Plasticity Index I_p	Effective Unit Weight γ (kN/m ³)
5	27	1.866	33.6	0.94	9.1	8.66

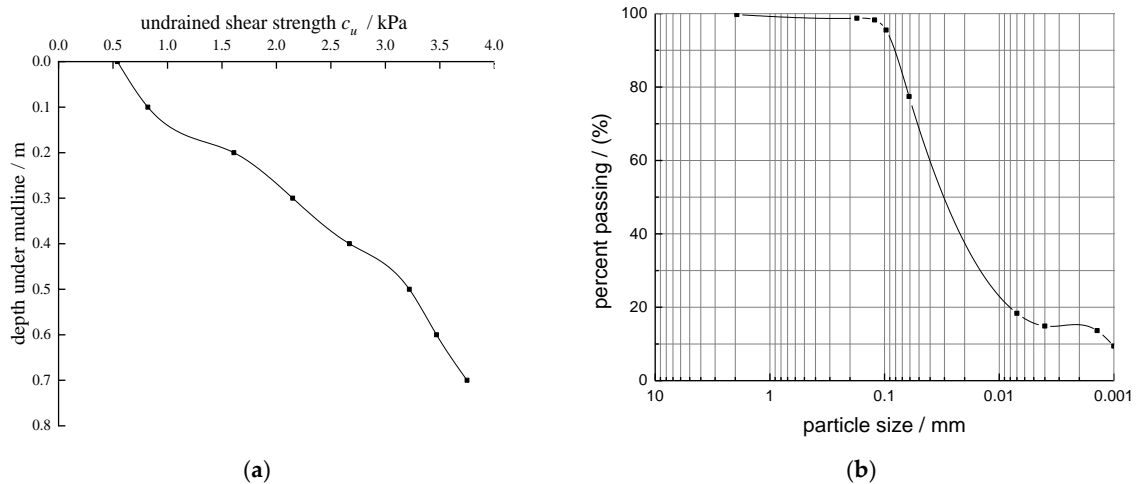


Figure 6. Soil parameters of model test: (a) undrained shear strength c_u along depth; (b) grain size distribution.

2.3.2. Data Processing

The strains were obtained by static strain gauges DH3815 and corresponding system DH3815N. The range of strain gauge is $\pm 20,000 \mu\epsilon$, and the highest resolution is $1 \mu\epsilon$. The pore pressure was continuously monitored by DAQLab 2005. A horizontal displacement sensor was arranged at the top strain gauge to record the horizontal displacement at mudline. The model of horizontal displacement sensor is MS-50, and the accuracy is 1% mm.

The loading process was applied in six stages by weights, and each level was 8.3 N, 21.05 N, 33.8 N, 46.55 N, 59.3 N, and 72.05 N. The interval between each load level is 1 h. With the measured strains, the bending moment curve can be calculated as follows:

$$M(z) = \frac{\epsilon EI}{a} \tag{7}$$

where ϵ : measured strains and a : outer diameter.

The displacement can be obtained by integrating Equation (7):

$$y(z) = \frac{1}{EI} \iint M(z) dz^2 \tag{8}$$

2.3.3. Result Analysis

The p–y curve for silt was given by Wang et al. [21]:

$$p = Ap_u \tanh\left(\frac{K}{p_u} y\right) \tag{9}$$

where $A = 1.26$.

With the given p–y curve and iterative solution above, the normalized horizontal displacement of each point of monopile under mudline was obtained. The deflection curve of monopile ($F = 46.55 \text{ N}$) is drawn and compared with the result of model test, which is shown in Figure 7.

The results of finite difference calculation are slightly larger than the model test, but the overall trend of numerical analysis is generally consistent with the model test. The error of depth of rotation point is less than 10 mm, and the maximum error of normalized horizontal displacement is no more than 0.04.

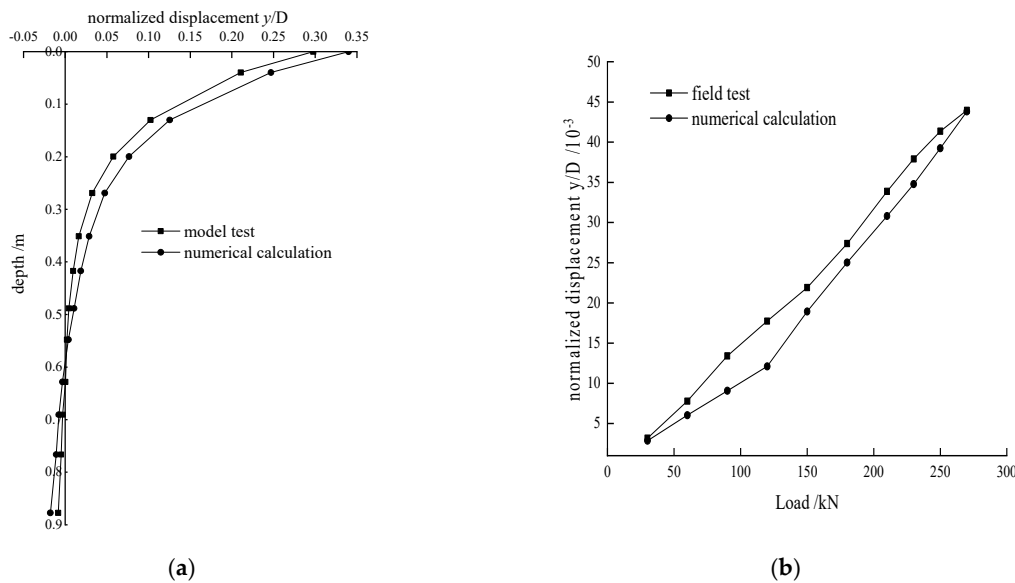


Figure 7. Displacement comparison. (a) Model test; (b) field test.

2.4. Verification with Field Test

The numerical results are verified by the field tests on lateral monotonic and cyclic loadings of offshore piles carried out by Zhu et al. [22]. According to the field test data, the p–y curves are imported into finite difference calculation program. It should be noted that the interior of pipe pile is filled with C30 concrete, and the top 0.9 m of pile length is deliberately not grouted for construction purposes, so it is critical to calculate the combined stiffness of steel pipe pile and concrete. If the stiffness is simply taken as steel pipe pile, the calculated stiffness will be smaller than the real combined stiffness, and the calculated displacement will be larger. In this paper, the combined stiffness is calculated by the method suggested by Kang et al. [23]. After the calculation, the displacement at the loading point under different level of loads is collected, and the calculated value is compared with the measured value, as shown in Figure 7b.

In order to simplify the calculation, it is assumed that the C30 concrete is grouted along the whole length of the pipe pile. Therefore, the displacement calculated is slightly lower, but close to the field data.

Through the comparison of numerical calculation results with model test and field test, it can be seen that, by selecting appropriate p–y curves, calculating iteratively through the finite difference method, the accuracy and reliability of displacement analysis is satisfied.

3. Consideration of Local Scour

To study the influence of local scour on monopile, the scour characteristic must be clarified, which is the basis and reference for the scour effect. On the basis of the Dafeng Offshore Wind Farm in Jiangsu Province, scour around large diameter monopile was surveyed and data including mudline altitude, erosion or deposition volume, maximum scour depth, and topographic fluctuation changes were collected. The water depth is 8~14 m, the wave height is 1~2 m, and designed pile outer diameter is 5.5 m. Besides pile 49#~52#, which were not investigated owing to weather conditions, a total of 68 sets of data were obtained.

3.1. Investigation Equipment

PDS software is used for navigation. The survey lines are arranged in the AutoCAD map, and then converted into navigation files. The positioning parameters and recording mode are set using the navigation software. Then, the depth sounder, locator, wave compensator, and computer are connected to guide the survey ship into the survey lines, and can locate and sound the measuring points according to the specified distance, and correct the course at any time according to the navigation software display. POSMV positioning system is adopted, which has the advantages of convenient operation and high accuracy. See Figure 8a for the position equipment.



Figure 8. Investigation equipment: (a) POSMV positioning system; (b) SeaBat T50-P multibeam bathymetric system.

Along with optical fiber compass, motion sensor, and professional underwater topographic mapping software, the SeaBat T50-P multibeam bathymetric system of Teledyne Reson company was used for survey, and real-time topographic changes in the whole field are obtained. The apparatus has an adjustable working frequency of 190 kHz~420 kHz, the detection angle can reach 165 degrees, and the sounding resolution is 6 mm. SeaBat T50-P multibeam sounding system is shown in Figure 8b.

3.2. Scour Characteristics

3.2.1. Range of Scour

The surveying range is 35 m in the center radius of the monopile. In the center radius of 17 m~35 m, the topographic fluctuation changes are very small (<1 m), and the average altitude is very close to the original designed mudline altitude (<0.1 m). The erosion or deposition are mainly concentrated in the range of 17 m from the center radius of monopile foundations, about 3D. The volume varies between -4307 m^3 and 199 m^3 , and the average value is -1983 m^3 . Except for the positive values of pile 7# and 65#, that is, deposition, the value of other monopile foundations is negative, that is, erosion. Figure 9a is the normal probability plot of erosion and deposition volume.

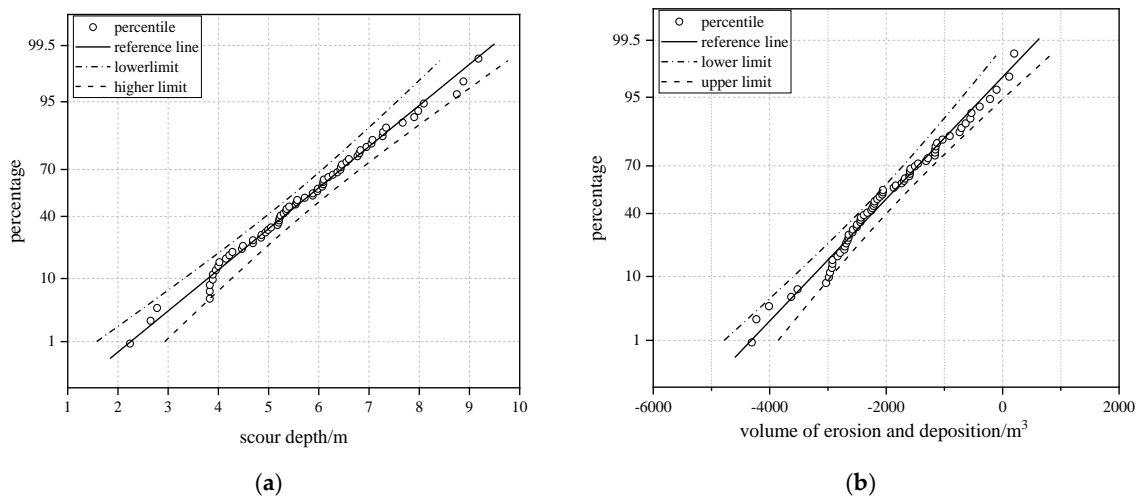


Figure 9. Normal probability plot. (a) Distribution of scour depth; (b) distribution of scour volume.

According to the scour depth obtained from 68 monopiles, the minimum is 2.24 m (0.41D), the maximum is 9.18 m (1.67D), and the average is 5.67 m (1.03D). The scouring depth is mainly concentrated in the range of 4 m~7 m, accounting for about 70% of the total number of monopiles. Figure 9b shows the normal probability of the distribution of maximum scour depth.

3.2.2. Pattern of Scour

(1) erosion in front and deposition behind

This pattern is typical for large diameter monopile. The morphology of local erosion and deposition around monopiles represents the majority in this survey, instead of regular scour pits. As shown in Figure 10a–d, the topography around the pile can be obviously divided into three parts: erosion area in front of the pile, deposition area behind, and symmetrical development area on the side.

Flow field changes because of monopile, and the velocity difference between the near bottom and the upper layer occurs; meanwhile, the water particles' movement produces a vortex system, which leads to erosion in front of the pile. Because monopile's diameter is much larger than the wavelength, the shield effect and diffraction will occur in the area behind the pile. The sediment carrying capacity of water flow here will be weakened, resulting in sediment deposition behind the pile. In the process of sediment transport on both sides of the pile foundation, affected by hydraulic and topographical conditions, whether it is erosion or deposition on the pile side may be unclear, but they have good regularity and generally develop symmetrically.

(2) annular scour with scour pit

A small number of monopiles showed another pattern, and the representative morphology is shown in Figure 10e,f. The shape of the scour pit is relatively regular, which is an inverted cone, and the lateral range of erosion and deposition is distributed in a circular manner. This pattern often occurs in the local scour around the long slender pile rather than monopile, and the topography differences may contribute to this result.

The results show that, except for a few obvious scouring pits around large diameter monopiles, most monopiles do not show regular scour pits, but rather local erosion and deposition.

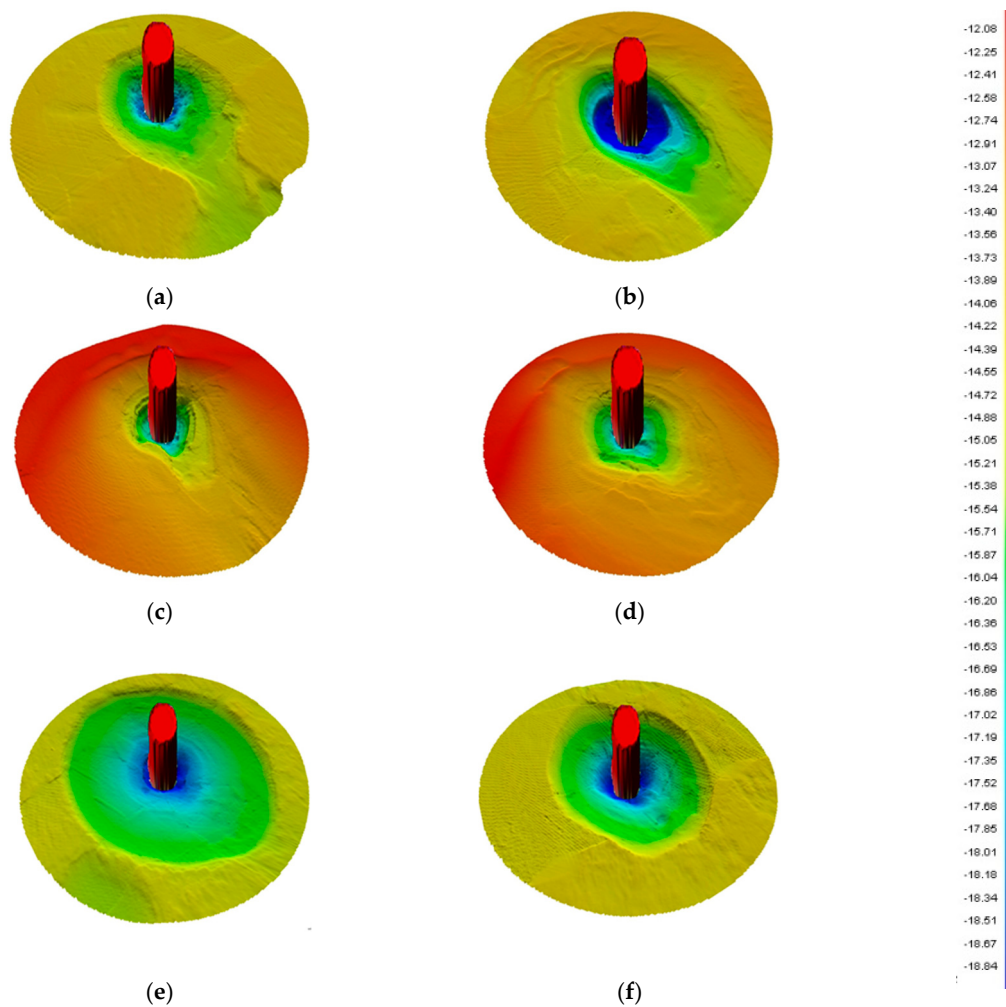


Figure 10. Scour patterns of large diameter monopile from Dafeng offshore wind farm in Jiangsu Province. (a–f) represent different monopiles.

3.3. Scour Effect

The most intuitive morphological changes are the erosion and deposition around pile and the scour pits. The traditional method in practical engineering is to reduce the embedment depth by removing a certain depth of soil according to the maximum scouring depth of scour pit [10,11]. This method is simple, but too conservative in design. The other method considers the slope angle, area, and other factors of the scour pit and introduces the stress history and wedge-shaped failure mechanism [12], which improves the accuracy, but it is complex in practical application.

More importantly, the method above is based on the appearance of scour pit, and only when the shape of scour pit is regular can it be more accurate. Generally, the small diameter piles can satisfy these conditions. However, from the previous summary, obvious scour pits only occurred in few monopiles, and there were no regular scour pits for most monopiles. If it is still approximate to the scour pit, the inherent errors will be introduced in determining the maximum scour depth, slope angle, and subsequent calculation. Therefore, the traditional method of simply removing soil layer is not suitable for large diameter monopile.

3.3.1. Morphological Features Equivalence

On the basis of the scour characteristics of large diameter monopile, this paper takes the volume of erosion and deposition as an equivalent criterion of morphological features, and converts it into the change of equivalent scour depth in a certain horizontal range. Assuming that the radius of scour

range is A , the erosion or deposition volume is V , and the pile diameter is D , the equivalent scour depth S_d can be calculated according to the following equation:

$$S_d = \frac{V}{\pi(A^2 - D^2)} \tag{10}$$

From the conclusion above, erosion and deposition are mainly concentrated in the center radius of $3D$, then Equation (10) can be rewritten as follows:

$$S_d = \frac{V}{8\pi D^2} \tag{11}$$

Taking pile 1#, 7#, 19#, 37#, 40#, and 57# as examples, equivalent scour depths are calculated by erosion and deposition volume, and the results are shown in Table 3. Compared with the maximum scour depth, the absolute error is 2.88 m~4.03 m, the minimum relative error is 40.9%, and the maximum relative error can reach 103.6%.

Table 3. Comparison between maximum and equivalent scour depth.

Pile Number	Scour Volume/m ³	Maximum Scour Depth/m	Equivalent Scour Depth/m	Absolute Error/m	Relative Error/(%)
1	-1602	-4.85	-1.97	2.88	59.4
7	113	-3.89	0.14	4.03	103.6
19	-1163	-5.05	-1.48	3.62	71.7
37	-2708	-6.83	-3.33	3. 05	51.2
40	-4307	-9.18	-5.30	3.88	42.3
57	-2931	-6.10	-3.61	2.49	40.9

3.3.2. Mechanical Properties Equivalence

Scour also changes the mechanical properties of soil, including the coefficient of consolidation degree, lateral earth pressure, void ratio, effective internal friction angle, and effective unit weight. Among them, the change of unit weigh is the largest, and other changes are relatively small [24]. In order to simplify the calculation, facilitate engineering application, and ensure sufficient accuracy, the stress history is taken as the mechanical equivalent criterion to modify the effective unit weight of soil in a certain longitudinal range. According to API, the influence is mainly within $6D$, so the soil unit weight after scour γ'_{sc} is as follows:

$$\gamma'_{sc} = \frac{6D}{6D - S_d} \gamma' \tag{12}$$

Taking pile 1# as an example, the pile length is 40 m, and the soil parameters used for calculation are listed in Table 4, where lateral load $F = 400$ kN, equivalent scour depth is 1.97 m, and the effective unit weight is corrected; the results are shown in Figure 11a–c. Compared with the traditional method of simply removing a certain depth of soil, the errors of maximum value of shear force, bending moment, and horizontal displacement are 16.2%, 10.6%, and 46.4%, respectively.

Table 4. Soil parameters of the construction site.

Soil Layer Number	Soil Name	Depth/m	Effective Unit Weight/(kN/m ²)	Friction Angle/(°)	Cohesion/kPa
1	Clay	0–2.4	7.6	2.3	4.5
2	Medium sand	2.4–6.1	8.1	23	0
3	Clay	6.1–15.9	7.8	3.5	9.7
4	Medium coarse sand	15.9–19.8	8.5	23	0
5	Sandy clay	19.8–21.4	9.3	13	30
6	Silty clay	21.4–	10.5	26	25

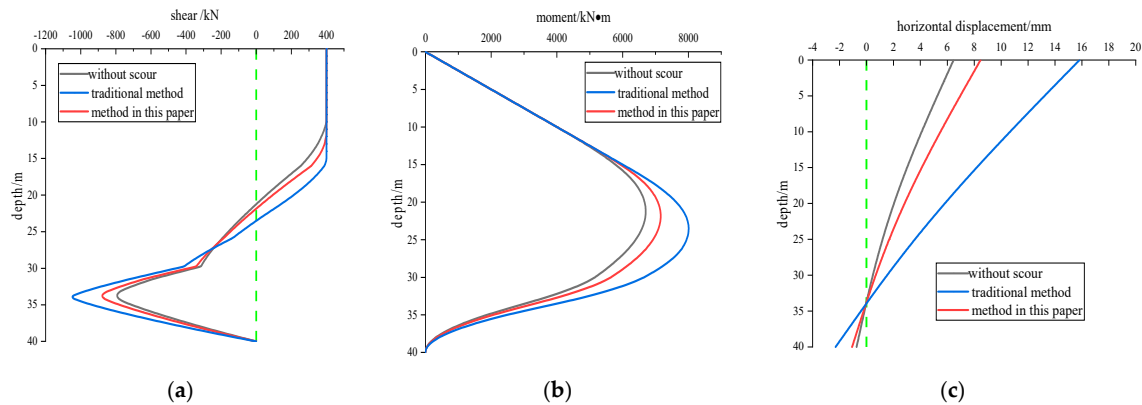


Figure 11. Deformation response calculated by different methods. (a) Shear force; (b) bending moment. (c) horizontal displacement.

4. Displacement of Large Diameter Monopile under Scour

The numerical analysis was verified in Section 2, and the scour effect was quantified in Section 3. By the proposed frame, on the basis of the data below, a finite element model was established in ABAQUS. The p–y curves for large diameter monopiles considering scour effect were obtained and then used to displacement analysis on large diameter monopiles under scour.

4.1. Model Parameters

The soil parameters in the construction site are shown in Table 4. The total length of the pile shaft is 40 m, and the embedment depth is 30 m. The outside diameter is 4 m and the wall thickness is 100 mm [25].

Zhang et al. [5] have verified that the isotropic hardening model can accurately predict the stress–strain behavior of saturated soil, so the Mises yield criterion and isotropic hardening model are adopted in this study. The initial and limiting yield stress were obtained by tri-axial CU test, and 15 sets of subsequent yield stress and corresponding strain were imported to ABAQUS to describe the strain-hardening in the stage of plastic. The three-dimensional model is meshed by eight-node hexahedron element and reduced integration and hourglass control is used in the analysis. A surface to surface interaction is created to simulate the pile–soil interaction. To avoid the boundary condition effect, the soil is 160 m in diameter and 60 m in height. The soil and pile interaction surface was idealized as frictionless. The grid within 24 m of monopile foundation is densified. The finite element model is shown in Figure 12a.

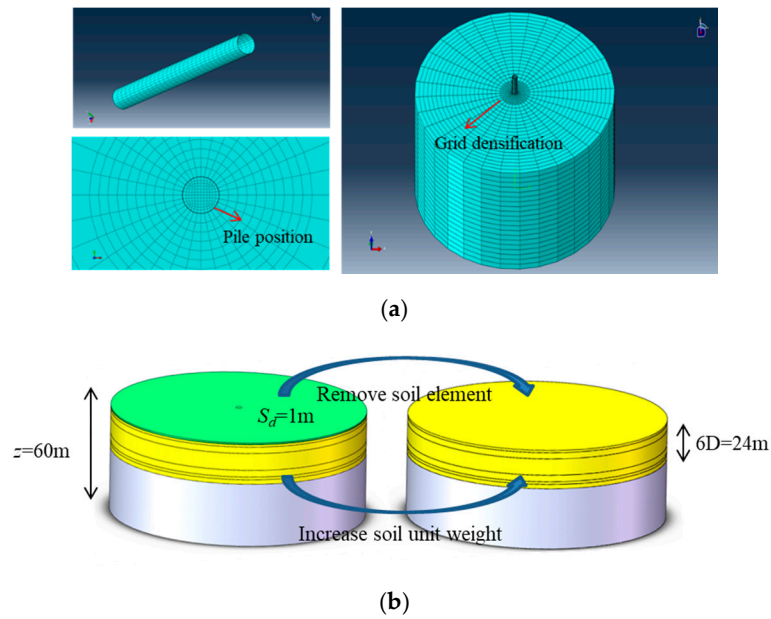


Figure 12. Finite element model established in ABAQUS. (a) Soil and pile model and grid densification; (b) remove soil element and increase γ' .

The equivalent scour depth was increased by 1 m each time, and the effective unit weight within $6D$ range was corrected correspondingly (Figure 12b), where the green part represents the equivalent scour depth of soil and the yellow part represents the soil layer to be corrected. P–y curves were extracted every 1 m. Figure 13 shows the p–y curves under different depths. According to the obtained p–y curves, the displacement was calculated every 1 m. The load acts on the pile head horizontally, and the direction is from left to right. The load is applied from 100 kN, increasing by 100 kN at each level and stopping at 600 kN. The results are collected and plotted in Figures 14 and 15.

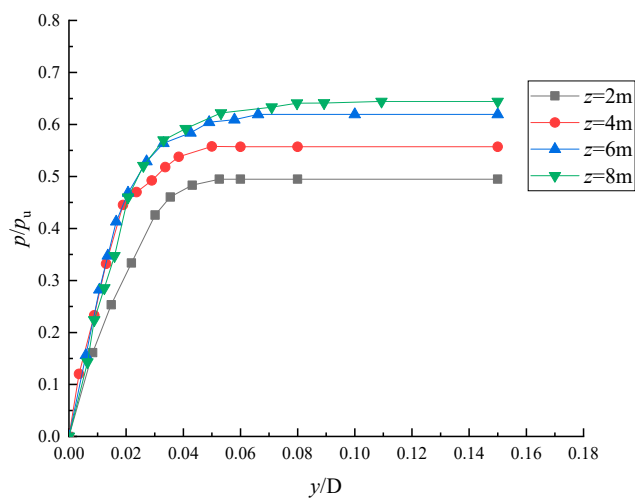


Figure 13. P–y curve under different depths.

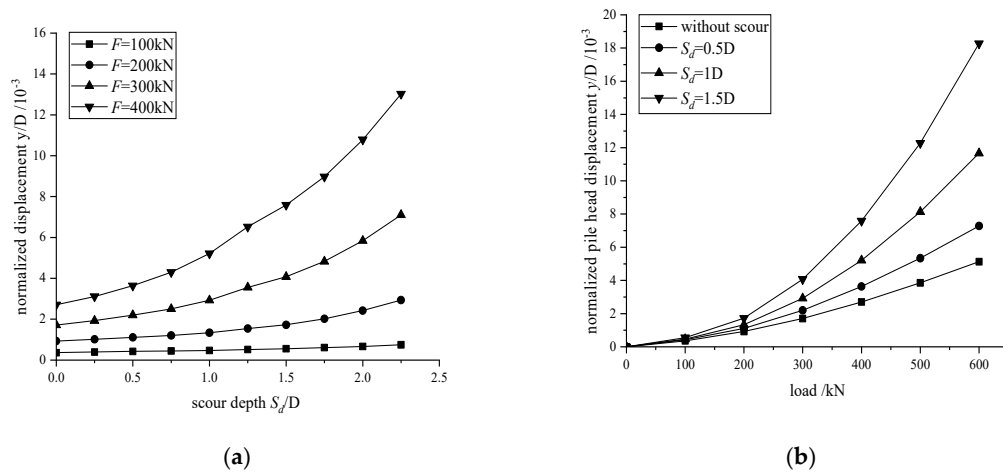


Figure 14. Pile head displacement of monopile under scour. (a) Scour depth–displacement under different load levels; (b) load–displacement under different scour depths.

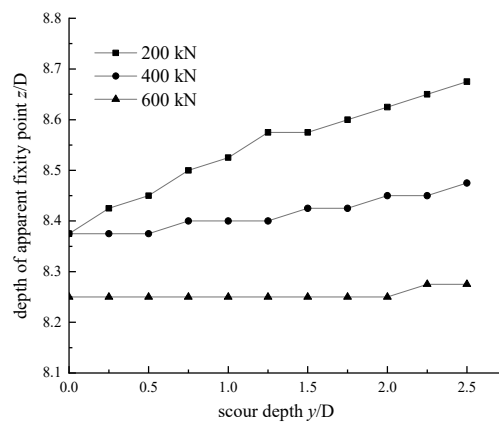


Figure 15. Scour depth–apparent fixity depth under different load levels.

4.2. Discussion

- (1) Figure 14a shows the relationship between scour depth and pile head displacement under each level of load. In the higher load level, with the increase of scour depth, the pile displacement increases nonlinear obviously; at the lower load level, the pile displacement changes little with the increase of scour depth, or can be approximately linear correlation.
- (2) It can be seen from Figure 14b that the displacement and load are nonlinear, whether or not scour occurs. When the load is less than 200 kN, the effect of local scour is not obvious. When the scour depth is 0.5D, the pile head displacement after scour can reach 1.4 times of that before scour. When the scour depth is 1.5D, it can reach 3.6 times of that before scour.
- (3) According to the position of the minimum positive and negative displacement, the point of apparent fixity ($y = 0$) could be determined by linear interpolation. Displacement under each level of load was collected. It can be seen from Figure 15 that the depth of apparent fixity decreases with the increase of scour depth. Taking the scour depth 2D as an example, when $F = 200$ kN, the apparent fixity depth increases by 1.2 m; when $F = 400$ kN, the depth increases by 0.4 m; and when $F = 600$ kN, the depth only increases by 0.1 m. In other words, the greater the load, the smaller the impact of scour on the apparent fixity depth. That is to say, at a high load level, scour has less influence on the apparent fixity depth. At a low load level, scour has a greater influence on the apparent fixity depth. This is because, at a high load level, the soil deformation has been fully developed and the pile displacement and rotation are mainly affected by the amplitude of load, so the influence of scour is relatively limited, thus the depth of apparent fixity

has no obvious change under scour. Meanwhile, at a low load level, the soil deformation is small, and scour deteriorates the soil conditions and reduces the embedment depth; thus, compared with load amplitude, scour also has a great influence on the depth of the apparent fixity.

5. Sensitivity of Pile Head Displacement under Scour

The increase of pile diameter, embedment length, and wall thickness can reduce the displacement of monopiles, but the variation characteristics under scour are not clear. For example, the horizontal displacement can be reduced by altering a certain pile parameter, but its effect may be greatly reduced under scour, which decreases the economy and safety of monopile foundations. Therefore, in this section, by discussing the relationships between pile head displacement, pile parameters, and scour depth, the sensitivity of displacement under scour is studied. This is how the analysis is realized: keeping the scour depth fixed to study the relationship between pile head displacement and pile parameters; and keeping the pile parameters fixed to study the displacement before and after scouring. To quantify the variation extent of horizontal displacement before and after scouring, the concept of scour sensitivity S is defined, which takes displacement as reference:

$$S = \frac{d_t}{d_0} \quad (13)$$

The value of S represents the susceptibility to scour. A higher value of S indicates a larger ratio of displacement after scour than that before scour, and that the parameter studied is more susceptible to scour. In the same way, a lower value of S indicates a smaller ratio of displacement after scour to that before scour, and that the parameter studied is less susceptible to scour.

According to Section 3, the average scour depth is $1.03D$, and in order to facilitate the comparison, all scour depths in this section are taken as $1D$. The initial pile diameter, embedment length, and wall thickness are 4 m, 40 m, and 100 mm, respectively. The value of pile parameters increases by 50% from the initial value, and the changes of displacement and scour sensitivity of pile head are compared. The load is applied to the top of the pile, with the amplitude of 600 kN and the direction from left to right.

5.1. Pile Diameter

The pile length and wall thickness of large diameter monopile is fixed, and the pile diameters of 4, 4.5, 5, 5.5, and 6 m are input in sequence. When the pile diameter increases from 4 m to 6 m, the horizontal displacement of pile head decreases from 47.7 mm (11.925×10^{-3}) to 26.9 mm (6.725×10^{-3}), which is 58% of the original value. The scour sensitivity decreased slightly from 2.35 to 2.23. The normalized displacement and sensitivity of pile head calculated under different pile diameters are shown in Figure 16. This illustrates that increasing the pile diameter will reduce the pile displacement, and the susceptibility to scour decreases slightly.

5.2. Pile Length

Figure 17 shows the normalized horizontal displacement and scour sensitivity of pile head under different pile lengths. The length of pile increases from 40 m to 60 m; the normalized horizontal displacement of pile head decreases from 11.925×10^{-3} (47.7 mm) to 4.55×10^{-3} (18.2 mm), becoming 38% of the original; and the scour sensitivity decreases from 2.35 to 1.34. It can be seen that increasing the pile length can significantly reduce the horizontal displacement of the pile body, and at the same time, the scouring sensitivity is also greatly reduced, which means the displacements are affected by scour to a lesser extent.

When the pile length reaches 50 m, the pile head displacement is 4.675×10^{-3} , and the scour sensitivity S is 1.37. After that, increasing the pile length will not lead to an obvious change of horizontal displacement and scour sensitivity, so it could be considered as a critical value.

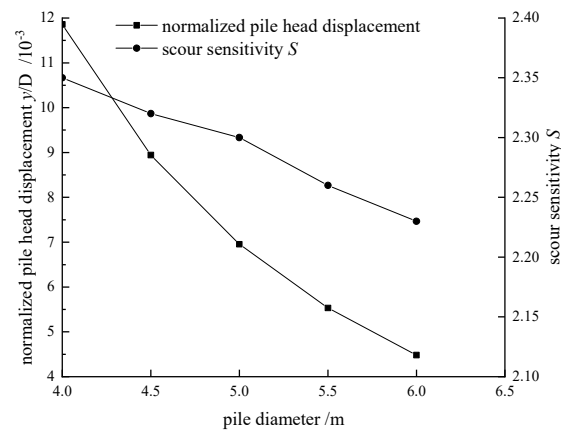


Figure 16. Pile displacement and scour sensitivity variation with pile diameter.

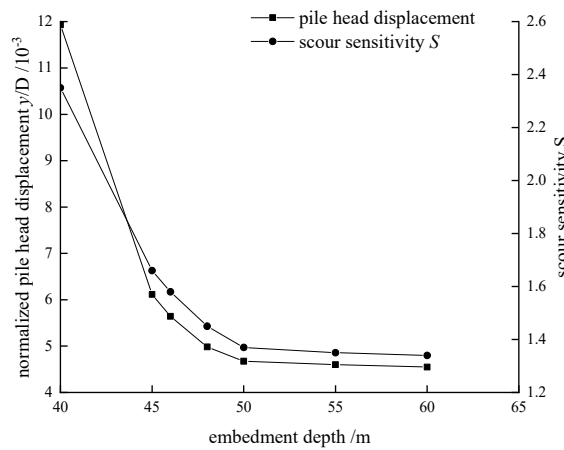


Figure 17. Pile displacement and scour sensitivity variation with embedment depth.

5.3. Wall Thickness

The influence of wall thickness on normalized pile head horizontal displacement under scour is shown in Figure 18. When the wall thickness increases from 100 mm to 150 mm, the displacement of pile head only decreases by 2.4 mm (0.6×10^{-3}), while the scour sensitivity increases from 2.35 to 2.42. That is to say, increasing the wall thickness has little effect on reducing the horizontal displacement and results in increased susceptibility to scour. So, increasing the wall thickness of monopiles to restrict the pile displacement is unreasonable when taking scour into consideration.

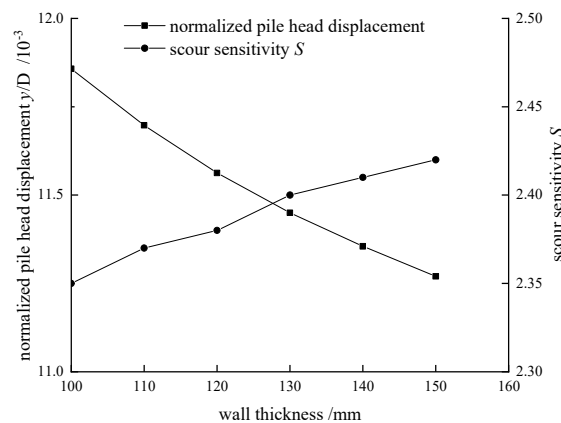


Figure 18. Variation of pile head displacement and scour sensitivity with pile wall thickness.

6. Conclusions

- (1) By selecting appropriate p–y curves from lab or field tests, calculating iteratively through finite difference program, the numerical frame introduced in this paper is feasible for the displacement analysis of large diameter monopile, and the accuracy and reliability of this method are satisfactory.
- (2) The scour characteristics were concluded by field data from Dafeng Offshore Wind Farm. The range of scour is mainly concentrated 17 m from the center radius of monopile foundations, about 3D. The maximum scour depth is 9.18 m (1.67D), and the average is 5.67 m (1.03D). Instead of regular scour pit, scour for large diameter monopile shows local erosion and deposition.
- (3) A new method applicable to large diameter monopile to take account of scour effect was proposed. In this study, the erosion or deposition volume and stress history were used as “memories” for the scour effect. Compared with the traditional method of simply removing a certain depth of soil, the errors of maximum value of shear force, bending moment, and horizontal displacement are 16.2%, 10.6%, and 46.4%, respectively.
- (4) P–y curves of large diameter monopile considered scour effect were obtained by ABAQUS. The deformation characteristics of large diameter monopile under scour were studied with the proposed numerical frame. With the increase of scour depth, the horizontal displacement of pile head increases nonlinearly. Under test conditions, the pile head displacement after scour can reach 1.4–3.6 times of that before scour. The depth of rotation point moves down with the increase of scour depth. At a high load level, scour has less influence on the rotation point depth; instead, scour has a greater influence at a low load level.
- (5) The relationships between pile head displacement, pile parameters, and scour depth are discussed. For different pile parameters, not only should the displacements be compared, the susceptibility to scour should also be evaluated. The analysis indicates that increasing the pile length is a more reasonable way than pile diameter and wall thickness to limit the scour effect on displacement of a large diameter pile. The definition of scour sensitivity is proposed, which may provide ideas for the design and analysis of monopile under scour.

Author Contributions: Z.W. conceived the study. Model test and field data of local scour were collected by H.L. (Hongjun Liu), and H.L. (Hao Leng) carried out tri-axial CU test. P–y curves and case study were analyzed by Z.W. R.H. gave some suggestions for manuscript writing. Y.B. and W.L. helped with plotting and page layout. H.L. (Hongjun Liu) supervised the whole study. All authors have read and agree to the published version of the manuscript.

Funding: This study was supported financially by the National Natural Science Foundation of China (grant no. 41572247).

Acknowledgments: Special thanks to China Power Investment Group and Huadian Heavy Industry Co., Ltd. for their generosity and support for scour monitoring.

Conflicts of Interest: The authors declare no conflict of interest.

References

1. Haiderali, A.; Madabhushi, G. Three-dimensional finite element modelling of monopiles for offshore wind turbines. In Proceedings of the World Congress on Advances in Civil Environmental and Materials Research, Seoul, Korea, 26–29 August 2012; pp. 3277–3295.
2. Wang, G.C.; Wang, W.; Yang, M. Design and analysis of monopile foundation for 3.6 mw offshore wind turbine. *Chin. J. Geotech. Eng.* **2011**, *33*, 95–100.
3. Bouzid, D.A. Numerical investigation of large-diameter monopiles in sands: Critical review and evaluation of both API and newly proposed p-y curves. *Int. J. Geomech.* **2018**, *18*, 1–21.
4. Achmus, M.; Terceros, M.; Thieken, K. Evaluation of p-y approaches for large diameter monopiles in soft clay. *Int. J. Offshore Polar Eng.* **2016**, *25*, 531–539.
5. Zhang, H.; Liu, R.; Yuan, Y.; Liang, C. A modified p-y curve method for offshore large-diameter monopile foundations. *J. Hydraul. Eng.* **2020**, *51*, 201–211.

6. Lee, M.; Bae, K.-T.; Lee, I.-W.; Yoo, M. Cyclic p-y curves of monopiles in dense dry sand using centrifuge model tests. *Appl. Sci.* **2019**, *9*, 1641. [[CrossRef](#)]
7. Liu, H.; Yang, Q. Influence of local scour on bearing performance of wind turbine supporting system. *Rock Soil Mech.* **2018**, *39*, 722–727.
8. Yang, B.; Wei, K.; Yang, W.; Li, T.; Qin, B.; Ning, L. A feasibility study for using fishnet to protect offshore wind turbine monopile foundations from damage by scouring. *Appl. Sci.* **2019**, *9*, 5023. [[CrossRef](#)]
9. Tseng, W.C.; Kuo, Y.S.; Lu, K.C.; Chen, J.W.; Chung, C.F.; Chen, R.C. Effect of scour on the natural frequency responses of the meteorological mast in the taiwan strait. *Energies* **2018**, *11*, 823. [[CrossRef](#)]
10. He, B.; Lai, Y.; Wang, L.; Hong, Y.; Zhu, R. Scour effects on the lateral behavior of a large-diameter monopile in soft clay: Role of stress history. *J. Mar. Sci. Eng.* **2019**, *7*, 170. [[CrossRef](#)]
11. Carswell, W.; Arwade, S.R.; DeGroot, D.J.; Myers, A.T. Natural frequency degradation and permanent accumulated rotation for offshore wind turbine monopiles in clay. *Renew. Energy* **2016**, *97*, 319–330. [[CrossRef](#)]
12. Dai, G.L.; Dai, H.; Yang, Y.H.; Gong, W.-M. Computation method and bearing characteristics of lateral bearing single pile foundation under scour condition. *China J. Highw. Transp.* **2018**, *31*, 104–112.
13. McClelland, B.; Focht, J.A. Soil modulus for laterally loaded piles. *Am. Soc. Civ. Eng. Trans.* **1958**, *123*, 1049–1063.
14. Matlock, H. Correlations for design of laterally loaded piles in soft clay. In Proceedings of the 2nd Offshore Tech Conference, Houston, TX, USA, 22–24 April 1970; pp. 577–594.
15. Reese, L.C.; Welch, R.C. Lateral loading of deep foundations in stiff clay. *J. Geotech. Geoenviron. Eng.* **1975**, *101*, 633–649.
16. Reese, L.C.; Cox, W.R.; Koop, F.D. Analysis of laterally loaded piles in sand. In Proceedings of the 6th Offshore Tech Conference, Houston, TX, USA, 6–8 May 1974; pp. 600–619.
17. API. *Designing and Constructing Fixed Offshore Platforms*; American Petroleum Institute: Dallas, TX, USA, 2014.
18. Wang, H.C.; Wu, D.Q.; Tian, P. A new united method of P-Y curves of laterally statically loaded piles in clay. *J. Hohai Univ. Nat. Sci.* **1991**, *1*, 9–17.
19. Wang, Z.Y.; Liu, H.J.; Hu, R.G. The review of p-y curve model for lateral cyclic loaded pile. *Mar. Sci. Bull. (Chin. Ed.)* **2020**, *39*, 401–406.
20. Yang, K.J.; Han, L.A. *Pile Foundation Engineering*; China Communications Press: Beijing, China, 1992.
21. Wang, T.; Wang, T.L. Experimental research on silt p-y curves. *Rock Soil Mech.* **2009**, *30*, 1343–1346.
22. Zhu, B.; Yang, Y.Y.; Yu, Z.G.; Guo, J.F.; Chen, Y.M. Field tests on lateral monotonic and cyclic loadings of offshore elevated piles. *Chin. J. Geotech. Eng.* **2012**, *34*, 1028–1037.
23. Kang, X.L.; Zhao, H.T.; Xue, J.Y.; Wu, J.B. Theoretic analysis for hooping mechanism and composite elastic modulus of CFSD members. *Eng. Mech.* **2007**, *24*, 121–125.
24. Lin, C.; Bennett, C.; Han, J.; Parsons, R.L. Scour effects on the response of laterally loaded piles considering stress history of sand. *Comput. Geotech.* **2010**, *37*, 1008–1014. [[CrossRef](#)]
25. Liu, R.; Yan, S.W. *Offshore Large Diameter Monoile Engineering*; China WaterPower Press: Beijing, China, 2016.

Publisher’s Note: MDPI stays neutral with regard to jurisdictional claims in published maps and institutional affiliations.



© 2020 by the authors. Licensee MDPI, Basel, Switzerland. This article is an open access article distributed under the terms and conditions of the Creative Commons Attribution (CC BY) license (<http://creativecommons.org/licenses/by/4.0/>).